

Borehole imagery of meteoric and marine ice layers in the Amery Ice Shelf, East Antarctica

Mike CRAVEN,¹ Frank CARSEY,² Alberto BEHAR,² Jaret MATTHEWS,² Russell BRAND,¹ Alan ELCHEIKH,¹ Seane HALL,³ Adam TREVERROW⁴

¹*Australian Antarctic Division and Antarctic Climate and Ecosystems CRC, Hobart, Tasmania 7001, Australia*
E-mail: m.craven@utas.edu.au

²*Jet Propulsion Laboratory, California Institute of Technology, 4800 Oak Grove Drive, Pasadena, California 91109-8099, USA*

³*Australian Antarctic Division, Hobart, Tasmania 7001, Australia*

⁴*IASOS and Antarctic Climate and Ecosystems CRC, Hobart, Tasmania 7001, Australia*

ABSTRACT. A real-time video camera probe was deployed in a hot-water drilled borehole through the Amery Ice Shelf, East Antarctica, where a total ice thickness of 480 m included at least 200 m of basal marine ice. Down-looking and side-looking digital video footage showed a striking transition from white bubbly meteoric ice above to dark marine ice below, but the transition was neither microscopically sharp nor flat, indicating the uneven nature (at centimetre scale) of the ice-shelf base upstream where the marine ice first started to accrete. Marine ice features were imaged including platelet structures, cell inclusions, entrained particles, and the interface with sea water at the base. The cells are assumed to be entrained sea water, and were present throughout the lower 100–150 m of the marine ice column, becoming larger and more prevalent as the lower surface was approached until, near the base, they became channels large enough that the camera field of view could not contain them. Platelets in the marine ice at depth appeared to be as large as 1–2 cm in diameter. Particles were visible in the borehole meltwater; probably marine and mineral particles liberated by the drill, but their distribution varied with depth.

1. INTRODUCTION

Most of the snow falling on the Antarctic continent drains via large ice streams and floating ice shelves to the sea, where it is lost either by iceberg calving or as basal melt beneath the shelves. The interaction between the base of ice shelves and the sea water circulating beneath them is complicated, with processes of basal freezing and melting occurring in different regions. The net output of these processes is important not only because it is a major component of the Antarctic mass budget, but because it also modifies the characteristics of the circulating sea-water masses. Cool, fresh Ice Shelf Water (ISW) from basal melting regions may mix with warmer, more saline Circumpolar Deep Water (CDW) on the continental shelf, influencing the formation of Antarctic Bottom Water, which plays a major role in global ocean circulation (Foldvik and Gammelsrød, 1988; Nicholls and others, 1991). In the Weddell Sea, changes in the characteristics of bottom water have occurred, with recent bottom water formation containing more glacial meltwater than in previous decades (Gordon, 1998). Phase change processes are sensitive to climate change, so that shifts in ocean temperatures and/or circulation patterns near Antarctica could lead to major modification of Antarctic ice shelves (Williams and others, 2002). Drastic losses have already been well documented for some of the smaller ice shelves in the Antarctic Peninsula region (Doake and Vaughan, 1991; Rott and others, 1996; Vaughan and Doake, 1996). The collapse of ice shelves could lead to accelerated discharge of the grounded ice, and is likely through glacio-eustasy to directly impact on global mean sea-level variations (Rott and others, 2002; De Angelis and Skvarca, 2003).

Large-scale basal melting in the grounding zone of ice shelves can occur at rapid annual average rates up to tens of

metres per annum (Rignot and Jacobs, 2002). As much as half the continental ice entering the Amery Ice Shelf (AIS) system is removed through basal melting within 100 km of first becoming afloat (I. Allison, <http://www.gfi.uib.no/frisp/Rep14/allison.pdf>). Due to the pressure dependence of the freezing point of sea water (Millero, 1978), some of this cool fresh modified ISW mass, rising along the thinning basal draft of an ice shelf, produces frazil ice crystals in the water column that can in turn accrete to the underside, forming layers of marine ice up to several hundred metres thick (Lewis and Perkin, 1986; Jenkins and Doake, 1991). The production of marine ice beneath the AIS, first detected in ice cores retrieved during a 1968 wintering expedition (Morgan, 1972), results chiefly in the formation of two longitudinal bands oriented along the ice-flow direction in the north-central and northwestern parts of the shelf (Fricker and others, 2001).

Access to the ocean cavity beneath, as well as to the ice sequence through the thickness of ice shelves, has become almost routine with the advent of rapid borehole production using hot-water drill (HWD) systems. The technique has been described and successfully employed on the major Antarctic ice shelves, Ross (Browning and others, 1979; Koci, 1984), Ronne (Engelhardt and Determann, 1987; Nicholls and others, 1991) and Amery (Craven and others, 2004), as well as on ice streams in West Antarctica (Engelhardt and others, 1990). Glacier borehole photography was pioneered on Blue Glacier, Washington, USA, where basal sliding velocities were measured directly to supplement velocities inferred from borehole inclinometry measurements (Harrison and Kamb, 1973; Engelhardt and others, 1978). Photographic imagery (including television footage) through ice-shelf access boreholes was first obtained during the Ross Ice Shelf Project, intended principally

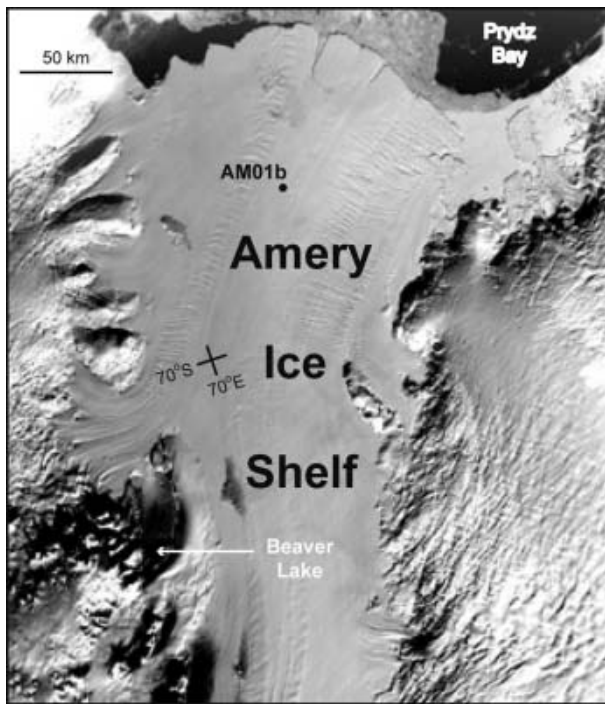


Fig. 1. Map of northern half of the AIS, and AM01b borehole location. Local snowfall accumulates over this part of the shelf ($300\text{ kg m}^{-2}\text{ a}^{-1}$ at the drill site). Further south the shelf passes through a superimposed- and bare-ice ablation zone with continental ice exposed at the surface.

to study the sub-shelf water column and sea-floor in search of marine and benthic life-forms (Bruchhausen and others, 1979; Lipps and others, 1979). A purpose-built Jet Propulsion Laboratory, California Institute of Technology, (JPL-CalTech) video camera system mounted in a pressure housing for real-time acquisition of in situ ice data has since been deployed on Kamb Ice Stream (former Ice Stream C), West Antarctica, capturing footage of isolated clasts embedded in the ice, debris strata, the solid base of the ice stream, a subglacial water-filled cavity, and the till bed over which the stream flows (Carsey and others, 2002). Here we present selected images through the ice sequence of the AIS, collected using the same real-time video camera probe, to examine ice structure in the north-central region of the shelf.

2. FIELD OPERATIONS

As part of the Amery Ice Shelf Ocean Research project (AMISOR), conducted by the Glaciology Program of the Australian Antarctic Division, a modular HWD system was deployed in December 2003 to melt an access borehole through a location 100 km from the centre of the iceberg calving front of the AIS, AM01b ($69^{\circ}25.9'\text{ S}$, $71^{\circ}26.8'\text{ E}$; Fig. 1). The resulting borehole had a nominal diameter of 300 mm through some 480 m of ice thickness, the lower 200–210 m of which was known to consist of accreted marine ice (Morgan, 1972; Craven and others, 2004).

A HWD coring head (Engelhardt and others, 2000) was deployed in the borehole during drilling to sample the ice at targeted depths. The core drilling proved difficult, with small irregular ice samples only retrieved at nominal depths of 250 m (within the meteoric ice) and 275 m (in the upper marine ice). The shelf was subsequently penetrated with the

HWD, the entire borehole reheated with a reaming head, and upon completion of integrity tests the JPL-CalTech borehole camera probe was used to record the ice sequence from top to bottom. Descent rates were typically in the range $0.02\text{--}0.06\text{ m s}^{-1}$. Due to the nature of the fibre-optic winch cabling arrangement (Carsey and others, 2002), the borehole was sampled in four approximately 120 m sections over a total period of ~ 12 hours. The probe was also allowed to descend a further 360 m to the ocean floor to examine the characteristics of the seabed (the depth counter reading ~ 30 m more than this due to the probe being swept sideways by strong sub-shelf currents). About 6 hours of digital video footage on each of the down-looking and side-looking video cameras was recorded to tape for later analysis, whilst regions of special interest were able to be investigated in greater detail due to the real-time surface station display capability of the system.

The fibre-optic cable from the winch to the borehole camera probe was fed over a sheave with a rotary encoder that sent a depth count signal to the recording electronics. The cable also looped over the capstan wheel on the HWD stand in order to guide the probe vertically down the borehole. This physical arrangement may have introduced a small counter error from the JPL-CalTech encoder, which has not been determined.

One of the major constraints on sampling with HWD access through cold ice is refreezing of the borehole over relatively short durations, even though it may be months before an undisturbed temperature profile is fully restored to the ice (Nixdorf and others, 1994). This limits the time available for sampling after warming of the water within the borehole and ice in the immediate vicinity of the wall. The speed of descent of the camera was partially determined by the need to capture the entire ice sequence and evacuate the hole within a single continuous 12 hour period. We decided against acquiring the sequence in halves over two sampling periods separated by a warm reaming run, as this could have introduced the undesired effect of altering the borehole walls significantly between recordings. A drawback of the adopted approach is that whilst the recordings were quite satisfactory when viewed in video mode, because of the optical retention capabilities of the human brain, high-quality still image captures were not always obtained. This problem was exacerbated in the marine ice where strong reflective surfaces that allow the auto-zoom side-looking lens to remain in sharp focus were not always present.

3. IMAGES FROM THE ICE BOREHOLE CAMERA SYSTEM

A schematic cross-section of the ice-shelf structure at the borehole site is given in Figure 2 as a visual aid to the relative depth location of the features discussed below.

3.1. Meteoric ice (0–275 m depth)

Particles were visible in the borehole meltwater even at the very top of the water column. These may have been biogenic and/or mineralogic particles liberated by the drill from the marine ice and mixed throughout the water column by the turbulence associated with the withdrawal of various HWD instruments from the borehole. It seemed at first a little surprising that they did not settle quickly enough to clear the uppermost part of the meltwater column prior to deployment of the camera probe. However, video inspection of the

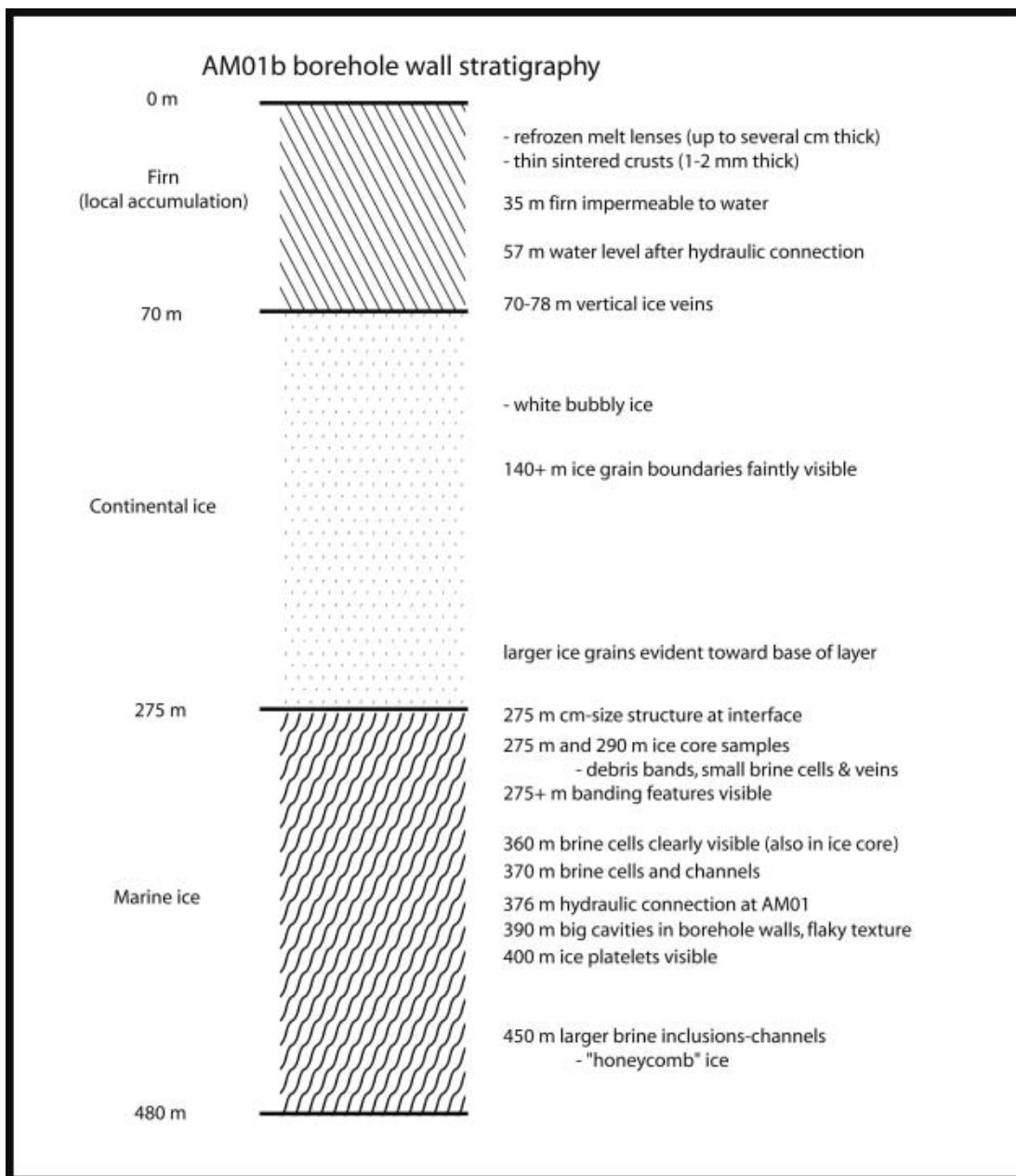


Fig. 2. Schematic cross-section of the three-layer ice-shelf structure at the borehole site.

incomplete borehole at 300 m depth showed that there was not only a patch of debris settled at the bottom of the hole, but also fine particulates suspended in the surrounding water, the particle size chiefly determining the rain-out rate. Close inspection of the side-looking video sequence also revealed the presence of occasional debris particles in the meteoric ice, particularly in the 140–160 m section. This may be related to an internal reflection layer detected in the vicinity of the borehole by Chinese ice radar surveys (personal communication from Wang Dali, 2004). It also indicates that at least some of the particulate matter in the upper borehole meltwater may have been sourced from aeolian dust deposits within the meteoric ice. This is likely to occur on the southern half of the AIS in the superimposed and bare-ice ablation zone with dust from the surrounding Prince Charles Mountains. Very few ice crystals were recorded in the upper water column, their occurrence identified by bright specular reflection of light from the

probe lamps. Their scarcity suggests that those observed were likely platelets freed from the borehole walls at depth, floating up through the water column, rather than products of local refreezing.

The meteoric ice sequence in the borehole consisted of ice from two distinct sources: 0–70 m, local near-coastal precipitation on the ice shelf between the Beaver Lake region and the borehole (Fig. 1), and 70–275 m, continental ice from the Lambert Glacier drainage basin; both well characterized by oxygen $\delta^{18}\text{O}$ stable-isotope values, -20‰ and -36‰ respectively (Morgan, 1972).

Refrozen ice lenses as thick as 20 mm were prevalent in the upper 70 m, formed from summer melt events in the firn. These were easily detected by the side-looking camera as layers of clear (darker) ice in the white granular and/or bubbly ice surrounding them (Fig. 3a). Thin (1–2 mm) ice lenses from surface wind-glazed crust events were also evident within this region (Fig. 3b). These are formed from

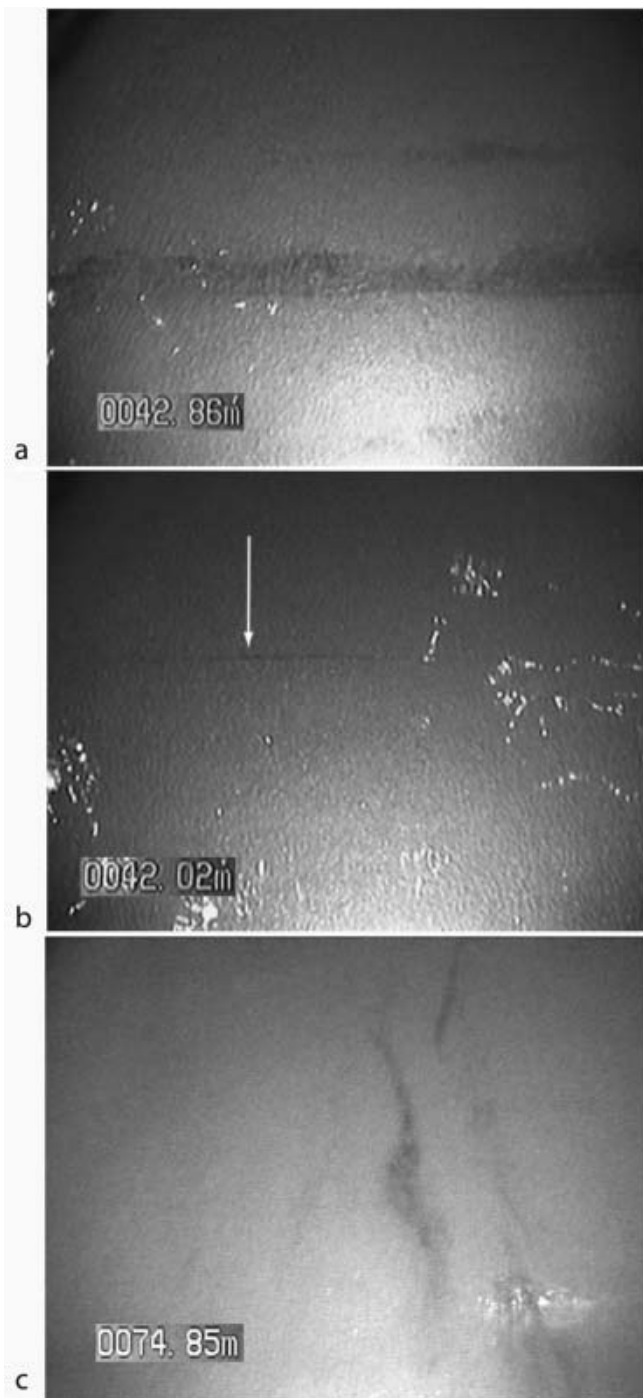


Fig. 3. (a) Thick 10–15 mm refrozen summer meltwater ice lens still preserved after the firn has compacted to bubbly glacial ice. (b) Thin (1–2 mm) wind-glazed crust ice lens (arrowed) preserved in granular bubbly glacial ice. (c) Vertical refrozen (2–10 mm thick) meltwater ice veins near the top of the continental ice layer. Note: all side-looking frames in this paper have had the image digitally inverted so that the top of the image is up in the ice. In the original recording by the probe, up in the image was down in the ice (Carsey and others, 2002).

the sintering together of ice grains at the surface during a precipitation hiatus with prolonged periods of strong wind across the ice shelf (Jones, 1983; Goodwin, 1988). Such crusts are generally opaque, relative to the transparent lenses formed by summer melting and refreezing events, though this property was impossible to distinguish from the video frames.

Prominent vertical ice veins were recorded in the ice in the 70–78 m depth range, most likely the result of meltwater refreezing in surface fissures on the continental ice during transit through the superimposed- and bare-ice ablation zone on the southern half of the shelf (Fig. 3c). Ice crystal grain boundaries were faintly visible in the video footage below 140 m, with larger grain-sizes at greater depth in the meteoric ice.

3.2. Meteoric–marine ice interface (approximately 275 m depth)

The meteoric–marine ice transition depth recorded by the borehole probe was around 279 m, which was probably a slight overestimate. It was known from ice-core drilling in the region that the interface was slightly shallower than this (270 m: Morgan, 1972; 276 m: personal communication from Li Yuansheng, 2003). Short core pieces collected with a HWD coring head (Engelhardt and others, 2000) from the vicinity of 275 m at AM01b were found to be clear ice with minor debris inclusions, and thus of marine origin. This has been confirmed by subsequent stable-isotope $\delta^{18}\text{O}$ measurements with an average value of $+1.8 \pm 0.1\text{‰}$ (compared to -36‰ for the continental meteoric ice).

The meteoric–marine ice transition was not a microscopically sharp interface (Fig. 4), nor did it appear to be strictly horizontal, much like the undulating discontinuity extending over 10–20 mm depth reported for the Ronne Ice Shelf transition (Eicken and others, 1994). This implies some meso-structure to the ice-shelf base upstream where the marine ice first started to accrete to the underside of the shelf. Such fine structure may simply be the scalloped nature of the original meteoric basal ice, well known from observations of underwater keels and overturned icebergs, in which the first marine ice frazil crystals began to accumulate.

3.3. Marine ice (275–480 m depth)

The marine ice layer was characterized by a lack of air bubbles, making it appear dark and largely transparent in reflected light by comparison to the meteoric ice. The sparsity at times of well-defined reflective features in the marine ice caused the side-looking camera to lose focus and drop into ‘hunting’ mode, and a strong reverse ghost reflection of the lens itself from the probe hull window appeared in the field of view.

Some very small-diameter cells (≤ 1 mm), and irregular veins were detected in the ice-core samples collected from 275 m depth at the very top of the marine ice layer. These were most likely brine inclusions (Fig. 5), but were not obvious in the video recordings. These core samples were also found to contain entrained debris of both biogenic and mineralogic origin, as has been previously reported for marine ice layers on the underside of ice shelves (Morgan, 1972; Oerter and others, 1992), largely confined to strings or discrete near-horizontal planes (Eicken and others, 1994; Moore and others, 1994).

Video footage of the upper marine ice exhibited splayed banding, with the illumination source reflecting strongly off layered features within it (Fig. 6). These were mostly seen side-on, but a few were viewed directly along their central axes, appearing as rays emanating from a focal point deeper within the ice. These features may well be correlated with the debris planes detected in the upper marine ice-core samples from 275 m depth.

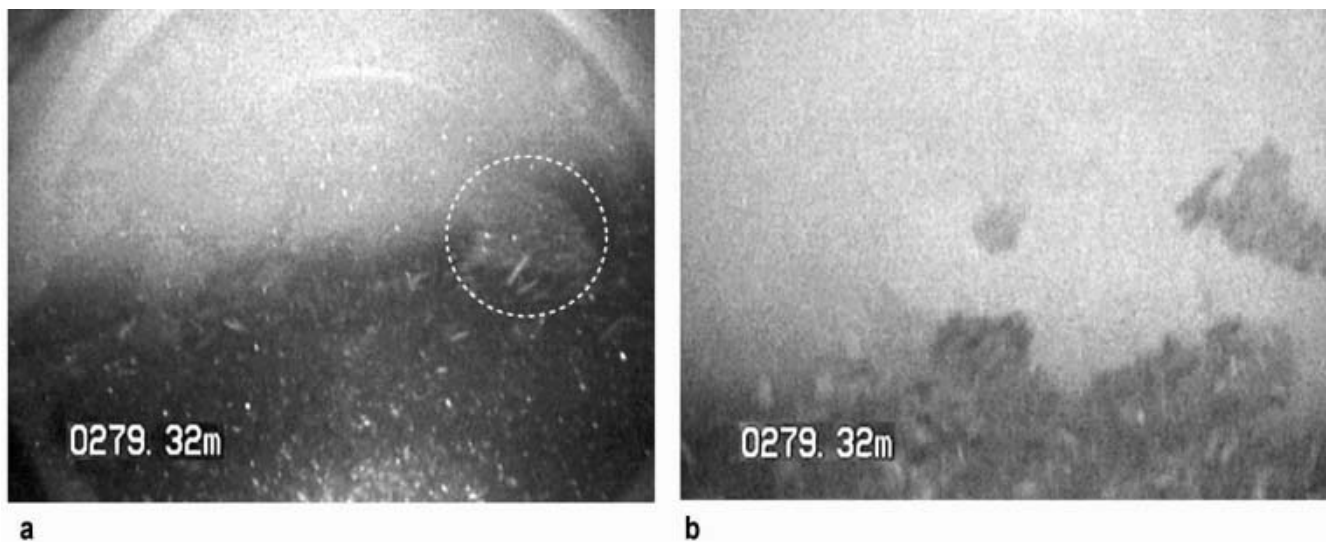


Fig. 4. Side-looking images at the meteoric–marine ice transition depth. (a) Tiny platelet crystals (2–5 mm across) appear in the dark marine ice immediately below the transition, and a much larger meteoric ice crystal grain projects into the marine ice across the interface (circled). Note camera lens reflection near top corners of the image. (b) The two dark patches (centre and middle-right) may be marine ice inclusions within the meteoric ice crystal matrix.

In January 2002 a HWD borehole and core sampling operation (AM01) took place at the same physical surface location on the AIS (within 250 m), where short ice-core sections were obtained at targeted depths within the marine ice layer. Thin-fabric analysis of the samples found banded rectangular facies in the 390 m core (Craven and others, 2004), which may relate to the banded layering recorded on video tape deep within the marine ice at AM01b (Fig. 7). Similar banded facies marine ice has been observed in core samples from the Hells Gate (74.8° S, 163.7° E) and Nansen (74.8° S, 162.8° E) ice shelves in Terra Nova Bay, with the suggestion that such strongly aligned *c*-axes fabrics were indicative of individual frazil crystals orienting nearly parallel to the ice–ocean interface during initial freezing

under the influence of boundary layer currents (Tison and others, 1993; Khazendar and others, 2001).

The borehole probe at AM01b showed that, from around 350 m down, small cells appeared in the marine ice layer, many of which were spheroidal with flattened bases covered by debris deposits (Fig. 8a). These are presumed to contain brine, concentrated remnants of trapped interstitial host water from frazil ice compaction processes at the base of the shelf. Their sphericity is the result of surface free energy minimization with the freezing of larger brine cells, and metamorphism during downward pore migration (very slow: at most 2 mm a^{-1}) under small vertical temperature gradients within the marine ice layer (Eicken and others, 1994). Ice-core samples collected at depths of 290, 360 and 390 m

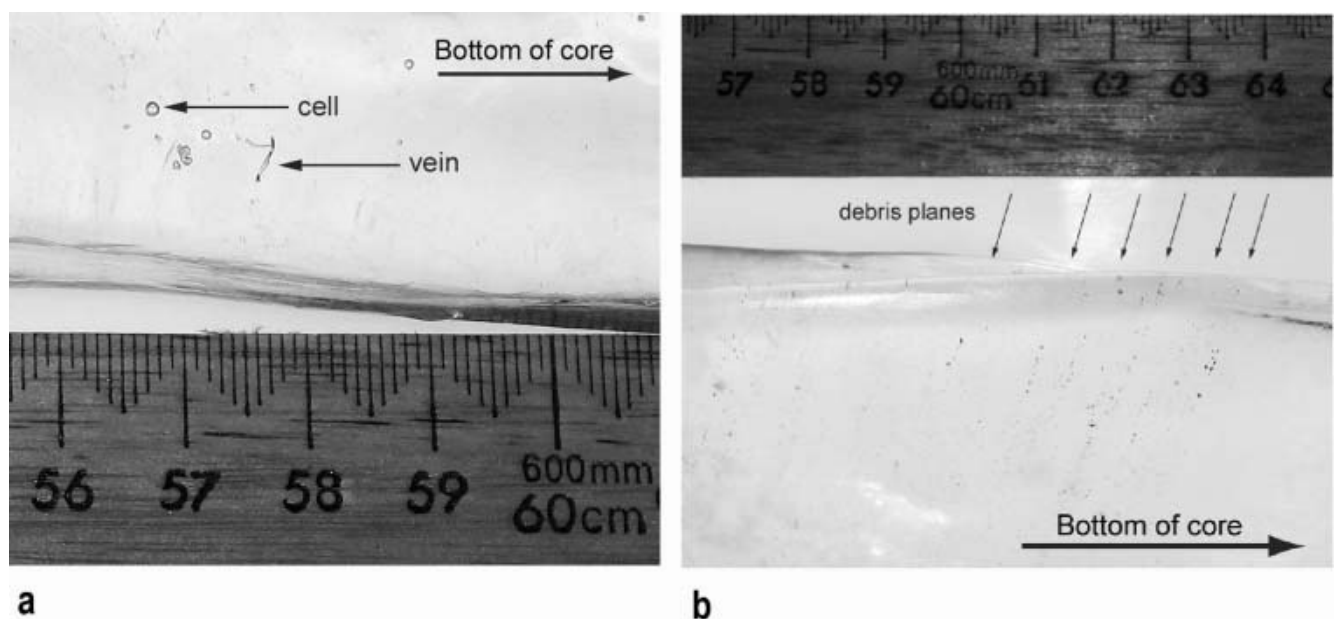


Fig. 5. Small ice-core sample obtained from 275 m at very top of marine ice layer with (a) small brine cells and veins that have not been clearly detected in video footage, and (b) debris planes that show up as banding on video.

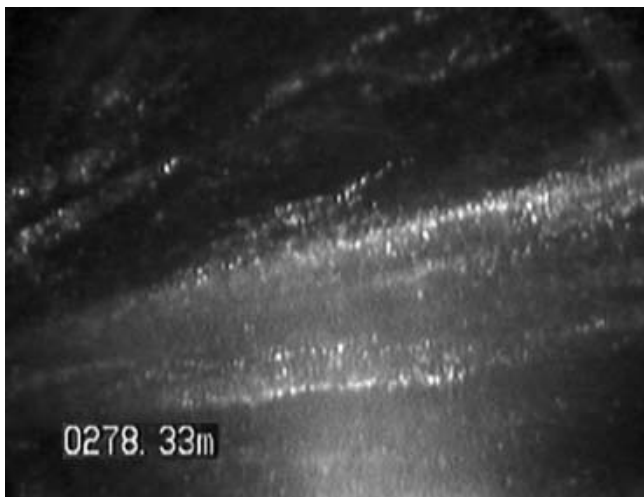


Fig. 6. Splayed banding in the upper marine-ice video footage, which is likely a manifestation of the debris planes evident in the ice-core sample obtained from similar depth.

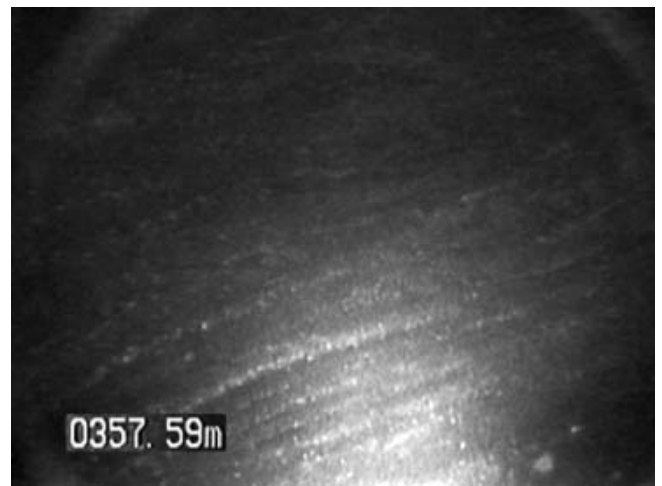
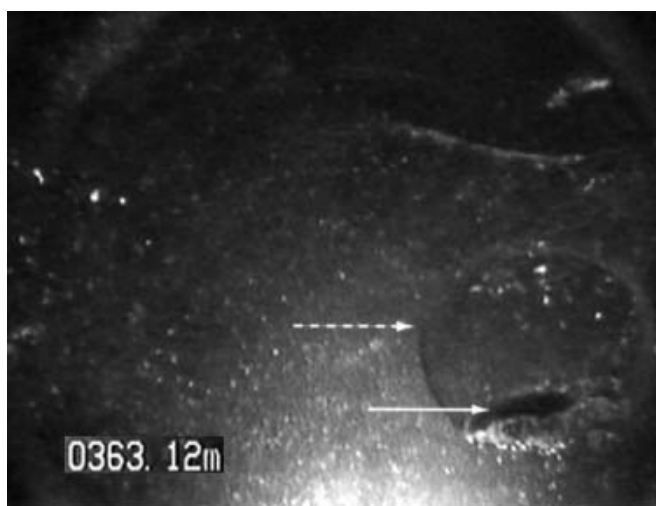


Fig. 7. Banded layering in the deeper marine ice. Apparent curvature may be an artefact of differential melting of the borehole wall during drilling and/or reaming.

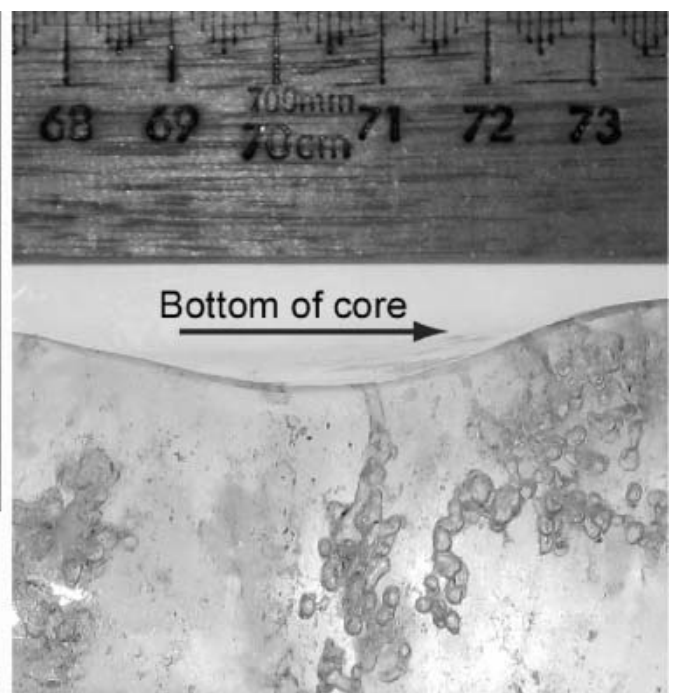
from the 2002 AM01 borehole were found to exhibit increased average bulk salinities with depth (0.06‰, 0.58‰ and 0.75‰ respectively), possibly indicative of increased volume and number of brine inclusions with depth (Fig. 8b). Discrete entrained debris particles were also evident alongside brine inclusions at great depth within the marine ice layer (Fig. 9).

The standard method to detect penetration of an ice shelf with a HWD is to monitor the pressure head in the subsurface recirculation supply well (Makinson, 1993). By deliberately maintaining the water level different to the height expected for a column of fresh water to be supported by the sea water below the shelf, it is possible to observe a well-head pressure-level change equivalent to several

metres over the space of a few seconds as initial breakthrough occurs. Whilst melting the AM01 borehole in 2002, the well-head sensor detected such a change with the drill head at 376 m depth, some 100 m above the true base of the shelf (confirmed at 479 m by borehole caliper re-entry upon completion of drilling). This was interpreted as being due to the 'honeycomb', or porous, nature of the marine ice layer allowing hydraulic connection with the ocean cavity through this thickness of ice (Craven and others, 2004). The weight of the fresh-water column in the borehole was sufficient to punch through a hydraulic connection, even though the cavities in the marine ice may not have been fully interconnected throughout the bottom 100 m of the layer.



a



b

Fig. 8. (a) Spheroidal brine cell showing cell wall (dotted arrow) and debris settled at base (solid arrow), and (b) similar brine inclusions (3–4 mm across) in the irregular shaped 360 m ice-core sample obtained from the associated drill site AM01.

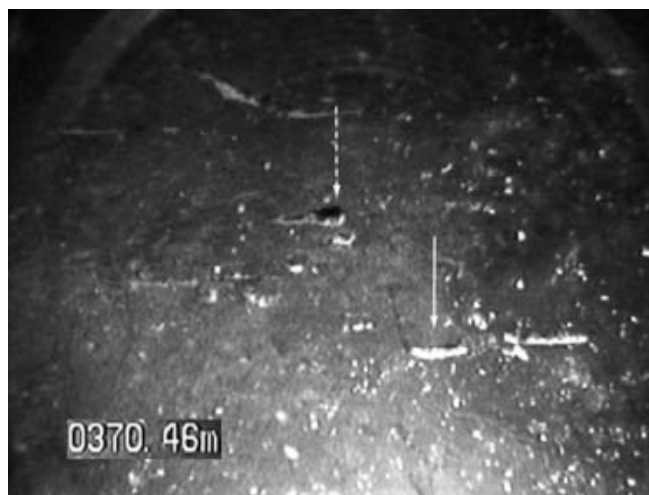


Fig. 9. Brine cell or bubble with fine debris settled at base (solid arrow), and discrete entrained debris particle (dashed arrow).

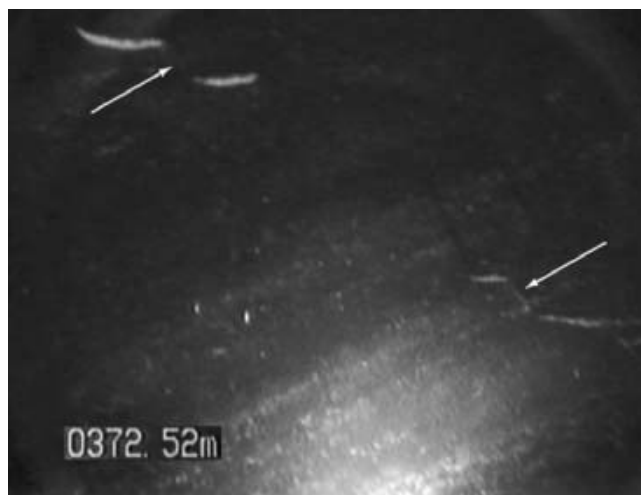


Fig. 10. Pairs of brine cells joined by steps (arrowed) to form larger brine inclusions, with brine channels also becoming prevalent from around this depth.

As the camera probe descended through the marine ice sequence, it was observed that a number of these features were conjoined to form larger brine cells, continuing up to the scale of brine channels (Fig. 10). The increased prevalence of such features around this depth (370 m) most likely accounts for the hydraulic connection with the sea water in the cavity beneath the shelf at AM01. Such a connection was not observed in the AM01b borehole due to failure of the well-head depth sensor earlier in the operation.

The discrete cells higher up in the older marine ice (ages decrease with depth) were probably once larger brine cells and channels, that have shrunk over time as more of the sea water within them has frozen. They therefore had prior access to scavenging a larger volume of sea water, which may well account for the large quantity of settled debris at their bases. Very few spheroidal cells were seen with little or no settled debris within them.

The mechanism proposed for the production of marine ice layers has two basic stages: individual frazil ice crystals

form in the water column, and then compact and consolidate at the base of the ice shelf; ice does not freeze in situ (Engelhardt and Determann, 1987; Oerter and others, 1992; Eicken and others, 1994; Tison and others, 2001). The visible structure of the marine ice at depth would seem to strongly support this mechanism, with individual platelet crystals clearly visible around 400 m (Fig. 11a). The common, near-horizontal orientation of platelets (Fig. 11b) over much of this region probably corresponds to the rectangular banded facies observed in the 390 m deep core sample from AM01.

3.4. Base of ice shelf (480 m depth)

Towards the base, little debris was evident within the borehole meltwater, in the marine ice or settled on the many ledges (formed by brine cells and/or uneven melting of the borehole walls). This could indicate that sea-water flushing of interconnected cavities at depth has been able to remove most of the debris that might otherwise have collected there.

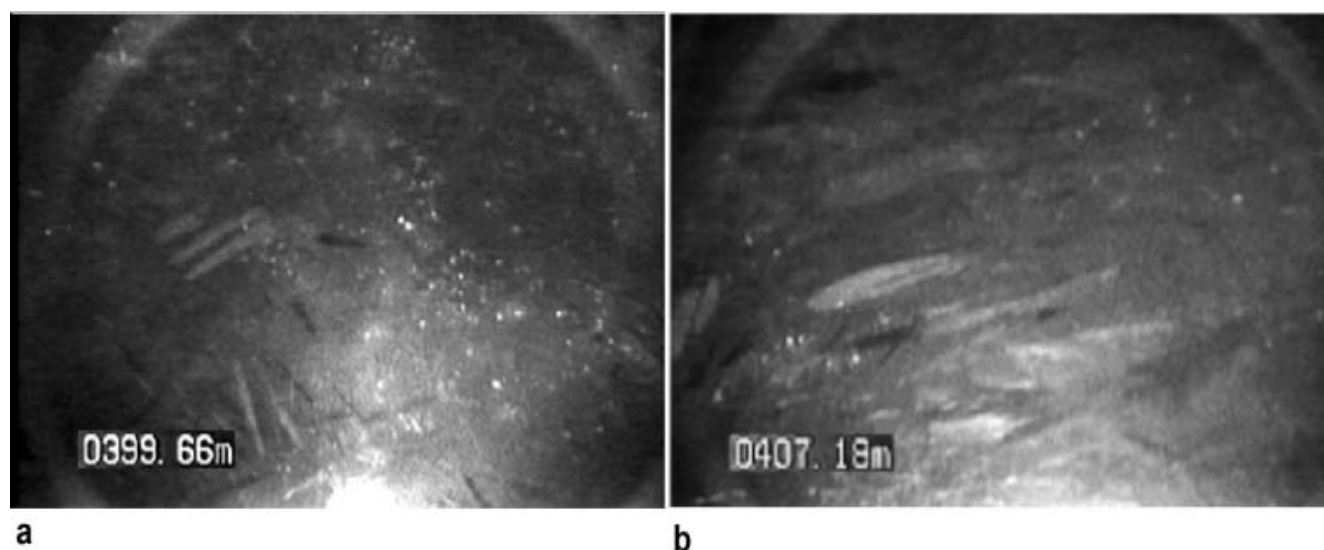


Fig. 11. Ice platelets with quite random orientation (a), and with mostly common orientation (b) in the marine ice matrix near 400 m depth.



Fig. 12. Large borehole wall cavity (upper half of image) in the marine ice layer at depth. The ledge in the lower half of the image has neither settled nor entrained debris evident here.

If so, the debris settled in brine cells higher in the marine ice comes from different source water that had a greater debris load further south under the shelf.

It proved exceptionally difficult to image the interface, around 480 m depth, between the marine ice and the underlying ocean with the side-looking camera. Problems were experienced trying to obtain and maintain focus as brine channel size and number increased toward the base (Fig. 12). The marine ice texture here presented a layered flaky appearance (Fig. 13), with ice platelets occasionally giving bright glints of specular reflection from the probe light source. A caliper profile from the AM01 HWD site in 2002 also indicated the irregular nature of the borehole walls in the final 100 m or so of the shelf (below the hydraulic connection depth). Exit images from the borehole into the ocean cavity were captured slightly better by the down-looking camera (Fig. 14). Video evidence suggests that the ice-shelf base interface with the sea water below may have open cavities yielding a large cellular or honeycomb structure, as distinct from unconsolidated slush that was

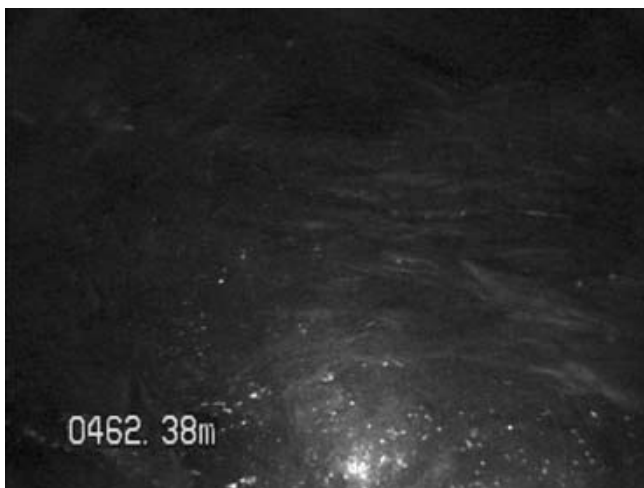


Fig. 13. The flaky layered texture of the marine ice (difficult to capture in still frames) showing a structural network rather than an aggregation of loose slush near the ice-shelf base.



Fig. 14. Indistinct exit cavity in the 'honeycomb' ice at the borehole base, as captured by the down-looking camera.

encountered at the base of the Ronne Ice Shelf, partially filling the lower 35 m of the borehole there (Engelhardt and Determann, 1987).

It remains unclear whether the ice shelf is undergoing basal melting or freezing at the site. Even the presence of ice crystals in the first 20 m or more of the water column immediately beneath the shelf (Fig. 15) may either be indicative of local freezing, or be the result of ice crystals being stripped from the irregular base of the shelf by the steady currents detected there (measured by current meter as $0.13 \pm 0.03 \text{ m s}^{-1}$). The small temperature gradient measured by a thermistor string installation through the base of the shelf in the AM01 borehole has not yet yielded conclusive results (Craven and others, 2004).

4. CONCLUSIONS

With the JPL-CalTech ice borehole camera probe we have been able to examine in situ the ice structure of the north-central AIS (site AM01b) within 100 km of the calving front.



Fig. 15. What are possibly small ice crystals (arrowed) swept by in the steady current immediately beneath the ice-shelf base (lens flare evident on left of image).

It was possible to detect three strata: local accumulation with horizontal ice lenses (0–70 m); bubbly continental ice with vertical veins in its upper regions (70–275 m); and accreted marine ice with embedded debris and brine cell inclusions (275–480 m). Thick summer melt lenses, and occasional thin wind crusts observed in the local accumulation layer may be a useful adjunct to ice-core annual-layer analyses.

Debris inclusions (in distinct planes and/or strings) were particularly prevalent in the upper part of the marine ice layer, with their diminution at depth likely a result of reduced debris load in the interstitial host water during frazil compaction at the base of the shelf closer to the site. The honeycomb nature of the ice, previously reported at depth from short core samples collected 2 years earlier at the same site, was observed *in situ* for the first time, revealing the presence of inclusions, in the form of spheroidal cells, and channels of what was probably concentrated brine in at least the lower half of the marine ice layer in the region. The interconnection of this network of brine features deep in the marine ice layer with sea water below makes the bottom 100 m of the shelf in this area particularly sensitive to any alterations to water temperatures and/or circulation patterns under global climate-change scenarios.

The presence of sea-water-filled englacial conduits in the marine ice at great depth may have significant ramifications for the modelling of ice-shelf rheology where thick layers exist. Typical surface glaciology and remote-sensing studies have not revealed their presence, and as the ice is very close to the local sea-water pressure-freezing temperature standard, core drill sampling may not be viable. The JPL-CalTech borehole probe is therefore a valuable tool for increasing our knowledge of significant marine ice deposits at the base of ice shelves.

ACKNOWLEDGEMENTS

The authors wish to acknowledge the support of personnel from the Australian National Antarctic Research Expeditions (ANARE) and the Australian Antarctic Division who have assisted with all stages of the AMISOR project. The Antarctic Ice Borehole Probe was developed at the Jet Propulsion Laboratory, California Institute of Technology, under a contract with the National Aeronautics and Space Administration. We would also like to thank NASA Headquarters, NASA's office of Earth Science, the US National Science Foundation Office of Polar Programs, and CalTech's Geological and Planetary Sciences Division for their support. Constructive reviews by D. MacAyeal and three other referees greatly improved the manuscript.

REFERENCES

- Browning, J.A., R.A. Bigl and D.A. Sommerville. 1979. Hot-water drilling and coring at site J-9, Ross Ice Shelf. *Antarct. J. U.S.*, **14**(5), 60–61.
- Bruchhausen, P.M., J.A. Raymond, S.S. Jacobs, A.L. DeVries, E.M. Thorndike and H.H. DeWitt. 1979. Fish, crustaceans and the sea floor under the Ross Ice Shelf. *Science*, **203**(4379), 449–451.
- Carsey, F., A. Behar, A. L. Lane, V. Realmuto and H. Engelhardt. 2002. A borehole camera system for imaging the deep interior of ice sheets. *J. Glaciol.*, **48**(163), 622–628.
- Craven, M. and 6 others. 2004. Initial borehole results from the Amery Ice Shelf hot-water drilling project. *Ann. Glaciol.*, **39**, 531–539.
- De Angelis, H. and P. Skvarca. 2003. Glacier surge after ice shelf collapse. *Science*, **299**(5612), 1560–1562.
- Doake, C.S.M. and D.G. Vaughan. 1991. Rapid disintegration of the Wordie Ice Shelf in response to atmospheric warming. *Nature*, **350**(6316), 328–330.
- Eicken, H., H. Oerter, H. Miller, W. Graf and J. Kipfstuhl. 1994. Textural characteristics and impurity content of meteoric and marine ice in the Ronne Ice Shelf, Antarctica. *J. Glaciol.*, **40**(135), 386–398.
- Engelhardt, H. and J. Determann. 1987. Borehole evidence for a thick layer of basal ice in the central Ronne Ice Shelf. *Nature*, **327**(6120), 318–319.
- Engelhardt, H.F., W.D. Harrison and B. Kamb. 1978. Basal sliding and conditions at the glacier bed as revealed by bore-hole photography. *J. Glaciol.*, **20**(84), 469–508.
- Engelhardt, H., N. Humphrey, B. Kamb and M. Fahnestock. 1990. Physical conditions at the base of a fast moving Antarctic ice stream. *Science*, **248**(4951), 57–59.
- Engelhardt, H., B. Kamb and R. Bolsey. 2000. A hot-water ice-coring drill. *J. Glaciol.*, **46**(153), 341–345.
- Foldvik, A. and T. Gammelsrød. 1988. Notes on Southern Ocean hydrography, sea-ice and bottom water formation. *Palaeogeogr., Palaeoclimatol., Palaeoecol.*, **67**(1–2), 3–17.
- Fricter, H.A., S. Popov, I. Allison and N. Young. 2001. Distribution of marine ice under the Amery Ice Shelf, East Antarctica. *Geophys. Res. Lett.*, **28**(11), 2241–2244.
- Goodwin, I.D. 1988. Firn core data from shallow drilling investigations in eastern Wilkes Land, East Antarctica. *ANARE Res. Notes* 65.
- Gordon, A.L. 1998. Western Weddell Sea thermohaline stratification. In Jacobs, S.S. and R.F. Weiss, eds. *Ocean, ice and atmosphere: interactions at the Antarctic continental margin*. Washington, DC, American Geophysical Union, 215–240. (Antarctic Research Series 75.)
- Harrison, W.D. and B. Kamb. 1973. Glacier bore-hole photography. *J. Glaciol.*, **12**(64), 129–137.
- Jenkins, A. and C.S.M. Doake. 1991. Ice–ocean interaction on Ronne Ice Shelf, Antarctica. *J. Geophys. Res.*, **96**(C1), 791–813.
- Jones, D. 1983. Snow stratigraphy observations in katabatic wind region of eastern Wilkes Land, East Antarctica. *ANARE Res. Notes* 17.
- Khazendar, A., J.-L. Tison, B. Stenni, M. Dini and A. Bondesan. 2001. Significant marine-ice accumulation in the ablation zone beneath an Antarctic ice shelf. *J. Glaciol.*, **47**(158), 359–368.
- Koci, B.R. 1984. Hot water drilling in Antarctic firn, and freezing rates in water-filled boreholes. *CRREL Spec. Rep.* 84-34, 101–103.
- Lewis, E.L. and R.G. Perkin. 1986. Ice pumps and their rates. *J. Geophys. Res.*, **91**(C10), 11,756–11,762.
- Lipps, J.H., T.E. Ronan, Jr and T.E. DeLaca. 1979. Life below the Ross Ice Shelf, Antarctica. *Science*, **203**(4379), 447–449.
- Makinson, K. 1993. The BAS hot water drill: development and current design. *Cold Reg. Sci. Technol.*, **22**(1), 121–132.
- Millero, F.J. 1978. Appendix 6. Freezing point of sea water. In *Eighth report of the Joint Panel on Oceanographic Tables and Standards*. Paris, Unesco, 29–31. (Technical Papers in Marine Science 28.)
- Moore, J.C., A.P. Reid and J. Kipfstuhl. 1994. Microstructure and electrical properties of marine ice and its relationship to meteoric ice and sea ice. *J. Geophys. Res.*, **99**(C3), 5171–5180.
- Morgan, V.I. 1972. Oxygen isotope evidence for bottom freezing on the Amery Ice Shelf. *Nature*, **238**(5364), 393–394.
- Nicholls, K.W., K. Makinson and A.V. Robinson. 1991. Ocean circulation beneath the Ronne Ice Shelf. *Nature*, **354**(6350), 221–223.
- Nixdorf, U., H. Oerter and H. Miller. 1994. First access to the ocean beneath Ekströmisen, Antarctica, by means of hot-water drilling. *Ann. Glaciol.*, **20**, 110–114.

- Oerter, H. and 6 others. 1992. Evidence for basal marine ice in the Filchner–Ronne Ice Shelf. *Nature*, **358**(6385), 399–401.
- Rignot, E. and S.S. Jacobs. 2002. Rapid bottom melting widespread near Antarctic ice sheet grounding lines. *Science*, **296**(5575), 2020–2023.
- Rott, H., P. Skvarca and T. Nagler. 1996. Rapid collapse of northern Larsen Ice Shelf, Antarctica. *Science*, **271**(5250), 788–792.
- Rott, H., W. Rack, P. Skvarca and H. De Angelis. 2002. Northern Larsen Ice Shelf, Antarctica: further retreat after collapse. *Ann. Glaciol.*, **34**, 277–282.
- Tison, J.L., D. Ronveaux and R.D. Lorrain. 1993. Low salinity frazil ice generation at the base of a small Antarctic ice shelf. *Antarct. Sci.*, **5**(3), 309–322.
- Tison, J.-L., A. Khazendar and E. Roulin. 2001. A two-phase approach to the simulation of the combined isotope/salinity signal of marine ice. *J. Geophys. Res.*, **106**(C12), 31,387–31,401.
- Vaughan, D.G. and C.S.M. Doake. 1996. Recent atmospheric warming and retreat of ice shelves on the Antarctic Peninsula. *Nature*, **379**(6563), 328–331.
- Williams, M.J.M., R.C. Warner and W.F. Budd. 2002. Sensitivity of the Amery Ice Shelf, Antarctica, to changes in the climate of the Southern Ocean. *J. Climate*, **15**(19), 2740–2757.

MS received 2 September 2004 and accepted in revised form 14 November 2004